2D non-linear gravimetric inversion to estimate basement relief and lateral variation of density contrast

Diego M. Novais[2], Joelson da C. Batista[1,2], Milton J. Porsani[1,2] – [1]UFBA/[2]INCT-GP

This paper was prepared for presentation during the 18th International Congress of the Brazilian Geophysical Society held in Rio de Janeiro, Brazil, 16-19 October 2023.

Abstract

This work proposes using a two-dimensional nonlinear inversion gravimetric methodology to infer the geometry of the boundary between the sedimentary deposit and its basement and the definition of the simulated lateral density contrast in the sedimentary basin environment. The interpretation model in question comprises a set of rectangular prisms in 2D space. The parameters estimated in the methodology inversion proposal are the thickness of each prism and your density contrast, interpreted in terms of the depth of the basement and the lateral variation of contrast between the basement and the basin sediment. In inversions commonly used to estimate the basement depth, the lateral density contrast is neglected. Still, this fact cannot be neglected due to the complex geological configurations present in the subsurface. This work proposes an inversion procedure considering this variation in density contrast. In this research, the inversion and its stability are validated through of study of regularization. The first study used a smoothness link of the basement relief and the regularization with a priori information. The second is from the use of both density and depth of the basement. The methods are tested with gravimetric anomalies from synthetic data for a better analysis of the behavior of this technique.

Introduction

In most cases, the methods to determine the sedimentary basin depth through the gravimetric anomaly do not consider a lateral variation of the density contrast between the basement and the overlying sediment. However, it is necessary to evaluate the lateral density contrast due to the complex geology of the basins with the presence of intrusions, salt diapirs, faults, and other geological events that are part of the formation process of a sedimentary basin. There are a large number of authors who estimate the depth of the density contrast without lateral variation, for the basement or the Moho discontinuity, among them Barbosa et al. (1997), Barbosa et al. (1999), Gòmez-Ortiz and Agarwal (2005), Silva et al. (2010) and Uieda and Barbosa (2017). Bastos and Oliveira (2020) estimate the depth of the basement and Moho discontinuity but insert multiple overlying layers differently from other authors.

The nonlinear gravitational inversion method to estimate the basement depth and the lateral variation of density contrast, implemented in this work, is based on the Gauss-Newton method, following a regularization strategy with two types of constraints: the smoothness applied to the basement depth and the equality with a priori information that can be used to both depth and lateral variation of density contrast. The work will analyze the behavior of the nonlinear inversion with the application of the different regularizations mentioned above and how this impacts the stability of the inversion. Tests with synthetic data will allow analyzing how reasonable the inversion estimates are about the parameters: basement depth and lateral variation of density contrast. Different synthetic models were analyzed, generating disturbances in the data and implementing regularizations to analyze the inversion algorithm.

Methodology

Assume that a set of discrete two-dimensional prisms with different densities and depths can model sedimentary basins composed of sediments and basements according to Figure 1. Let be a vector with N data set of gravitational

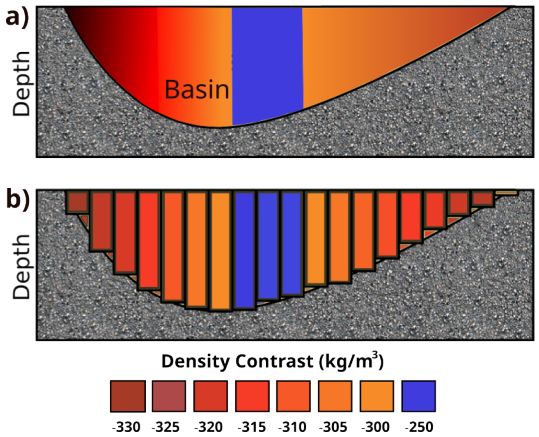

Figure 1: Modeling of a sedimentary basin through prisms, the variables being the depth and density of each prism. a) Model of a basin with a variation of basement depth and contrast between the density of sedimentary and basement layers. b) Basin modeling from a) in prisms (Adapted from Uieda, 2020).

anomalies produced by a sedimentary basin (Figure 1). Assuming that the basin has a depocenter, as shown in Figure 1a, and a variation in the density contrast between the sedimentary layers and the basement. One can approximate the interpretation model through a set M of prisms juxtaposed with the 2D dimension (Figure 1b). The

prisms are placed such that their type is aligned on the ground surface, and all prisms have the same width.

Considering the lateral variation of the prism density contrasts and the depth of the basement, the predicted gravitational anomaly to map the basement is a nonlinear function of the parameters z_j and $\Delta\rho_j$, $j = 1,...,M$.Let g_i be the set of observations of N Bouguer Anomalies produced by the relief of the basement and variation of the lateral contrast of the density of the sediments of a sedimentary basin. It assumed that possible regional effects and the residual Bouguer anomaly or simply Bouguer anomaly has been removed. The thickness of the prisms and the variation in the density contrast between the sedimentary layers and the basement are the parameters to be estimated and are related to g_i gravity through nonlinear relationships,

$$g_i = \sum_{j=1}^{M} F(p_j, r_i) \tag{1}$$

$$p_j = [z_j \;\; \Delta\rho_j]^T \tag{2}$$

where $F(p_j, r_i)$ is a non-linear function that produces gravimetric anomaly of a prism at position r_i, thickness z_j, and density contrast $\Delta\rho_j$ between the sediment and the basement (Silva et al.,2010).

For the nonlinear inverse problem with an estimation of z_j and $\Delta\rho_j$, we use the regularized Gauss-Newton method. Let $\mathbf{g}^o = \{g_1^o, g_2^o, ..., g_M^o\}^T$ be the vector of the observed gravity data and $\boldsymbol{g}$, whose i-th element of the vertical component of the predicted gravitational through Equation 1. To estimate the parameters to be inverted, producing predicted data as close as possible to the observed data, the objective function to be minimized

$$\tau(\boldsymbol{p}) = \Phi(\boldsymbol{p}) + \sum_{k=1}^{3} \mu_k \Psi_k(\boldsymbol{p}) \tag{3}$$

in Equation 3, μ_k is the weight assigned to the k-th regularization function $\Psi_k(\boldsymbol{p})$, $k = 1,...,3$ and $\Phi(\boldsymbol{p})$ is the misfit function given by

$$\Phi(\boldsymbol{p}) = \frac{1}{N} \|\boldsymbol{g}^o - \boldsymbol{g}\|_2^2 \tag{4}$$

where $\|\boldsymbol{g}^o - \boldsymbol{g}\|_2^2$ represents the Euclidean norm squared between observed and calculated data.

Two types of constraints are implemented for this inverse problem to be well-posed and have a stable solution. These constraints are introduced through regularization with two constraints: one for smoothness and one for equality. The smoothness bond is introduced with the application of Tikhonov's first-order regularization to the depth z_j (Ψ_1), as implemented in the works of Barbosa et al. (1997), Barbosa et al. (1999), Silva et al. (2006) and Bastos and Oliveira (2019). Data regularization with the incorporation of a priori data can be performed with depth z_j (Ψ_2) and density Δ_j (Ψ_3) information based on the work of Barbosa et al. (1997), Barbosa et al. (1999) and Bastos and Oliveira (2019). Mathematically, the regularizations of smoothness for z_j, equality with prior information for z_j and equality with prior information for $\Delta\rho_j$ are given by

$$\Psi_1(\boldsymbol{z}) = \|\boldsymbol{S}\boldsymbol{z}\| \tag{5}$$

where S is a 2(N-1)xM matrix given by,

$$\boldsymbol{S} = \begin{bmatrix} \boldsymbol{R} & \mathbf{0} & \mathbf{0} \\ \mathbf{0} & \boldsymbol{R} & \mathbf{0} \end{bmatrix}_{2(N-1)\times M}, \tag{6}$$

$$[\boldsymbol{R}]_{ij} \begin{cases} 1 & , j = i \\ -1 & , j = i+1 \\ 0 & , \text{otherwise} \end{cases}, \tag{7}$$

$$\Psi_2(\boldsymbol{z}) = \|\boldsymbol{A}\boldsymbol{z} - \boldsymbol{a}\|_2^2, \tag{8}$$

$$\Psi_3(\boldsymbol{\Delta\rho}) = \|\boldsymbol{B}\boldsymbol{\Delta\rho} - \boldsymbol{b}\|_2^2, \tag{9}$$

where A and B are $A \times M$ and $B \times M$ matrices, respectively, of which the k-th row has one element equal to one and all other elements equal to zero (Bastos e Oliveira, 2019). The location of the only non-zero component in the k-th row of A depends on the horizontal coordinate y_k A of the known thickness a_k. Now for the k-th line of B of the horizontal coordinate y_k B of the available density b_k. Let $\boldsymbol{z}$ be the parameter vector related to the prism's depth, basement, and sediment interface, and $\boldsymbol{\Delta\rho}$ be the parameter vector related to the density contrast of each prism.

Minimizing functional $\tau(\boldsymbol{p})$ given in Equation 3 concerning p is a nonlinear problem that will be solved iteratively. The standard procedure for performing this search iteratively starts with a particular initial approximation $\boldsymbol{p_0}$ and calculates a correction $\boldsymbol{\Delta p}$. This correction is then applied to the initial approximation giving rise to a new vector $\boldsymbol{p_1}$. This new vector is an initial approximation for calculating a second vector $\boldsymbol{p_2}$, and so on. The process ends when a vector $\tilde{\boldsymbol{p}}$ is found that minimizes the function in question. The Gauss-Newton method calculates the correction $\boldsymbol{\Delta p}$ starting with the Taylor series expansion up to the second order of the function to be minimized. Therefore, the calculation of the correction Dt is performed by solving the system of equations,

$$\begin{aligned}[\boldsymbol{J}^T\boldsymbol{J} + \mu_1\boldsymbol{\Psi}_1(\boldsymbol{z}) + \mu_2\boldsymbol{\Psi}_2(\boldsymbol{z}) + \mu_3\boldsymbol{\Psi}_3(\boldsymbol{\Delta\rho})]\boldsymbol{\Delta p} = \boldsymbol{J}^T[\boldsymbol{g}^o - \boldsymbol{g}] \\ - \mu_1\boldsymbol{\Psi}_1(\boldsymbol{z}) - \mu_2\boldsymbol{\Psi}_2(\boldsymbol{z}) - \mu_3\boldsymbol{\Psi}_1(\boldsymbol{\Delta\rho}),\end{aligned} \tag{10}$$

where $\boldsymbol{J}$ is the jacobian matrix of g_i (Equation 1).

Results

The results presented here were generated from simulated data from synthetic models of sedimentary basins. For the study of the behavior of the three regularization functions given, it was be implemented different configurations, with joint and isolated applications of the regularizations, to understand the behavior of the inversion in each of them. For the test, a pseudorandom noise with normal distribution with a size of 0.3 mGal was added to the observed synthetic data.

Models 1 and 2 of the basins in Figures 2 and 3 are adapted from synthetic models by Uieda (2020). Model 1 (Figure 1) presents a basin with a density contrast of $-300\,kg/cm^3$ along the entire basin. Model 2 (Figure 3) displays a model with a central density contrast of $-280\,kg/cm^3$, while the surrounding density contrast is $-300\,kg/cm^3$.

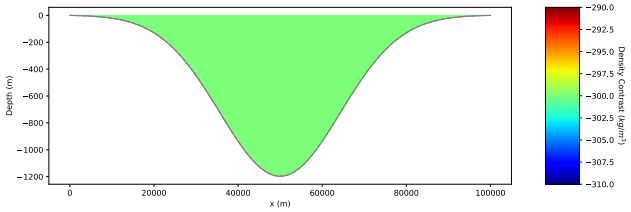

Figure 2: Model 1 of a synthetic basin with density contrast between basement and sediments $-300\,kg/cm^3$.

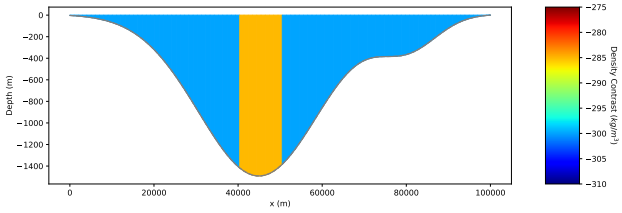

Figure 3: Model 2 of a synthetic basin with density contrast in the center of the basin between basement and sediments $-280\,kg/cm^3$ and in the surrounding regions of $-300\,kg/cm^3$.

Figures 4 and 5 show the results achieved through the inversion, respectively, of models 1 and 2 without a priori information, only smoothing for depth and density.

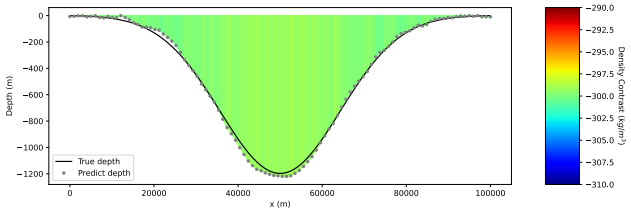

Figure 4: Density contrast data and basin depth of model 1 obtained through smooth inversion.

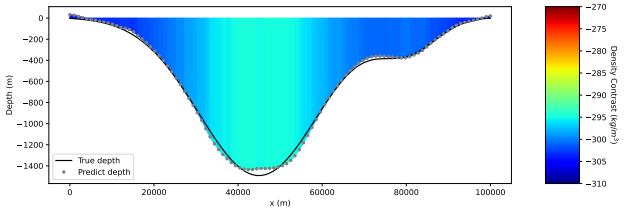

Figure 5: Density contrast data and basin depth of model 2 obtained through smooth inversion.

The graphs in Figures 6 and 7 illustrate the observed and predicted data through inversion. Figure 8 shows the predicted data for depth and density contrast with a priori density data and smoothness regularizations. Figure 9 chart displays predicted and observed data for model 2.

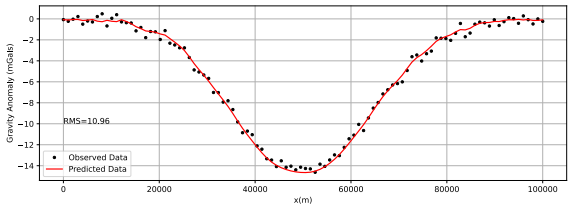

Figure 6: The graph presents the observed data (points) and calculated (red line) obtained through the smoothness regularized inversion of the density contrast and for depth related to model 1.

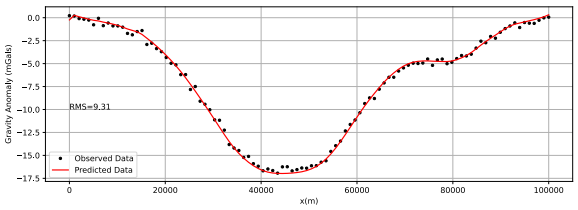

Figure 7: The graph presents the observed data (points) and calculated (red line) obtained through the smoothness regularized inversion of the density contrast and for depth related to model 2.

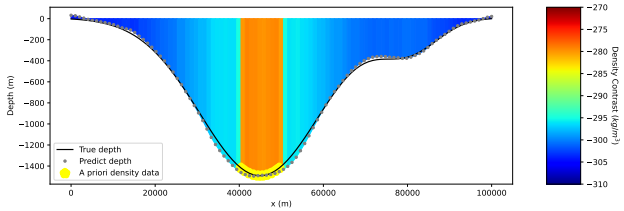

Figure 8: Density contrast data and basin depth of model 2 obtained through smooth inversion and a priori density contrast data represented by the points indicated in the figure.

It is possible to observe that, despite the inversion without the presence of a priori information identifying the anomalous density contrast in the center of the model 2, observing Figure 5, the data with a priori information resulted in a better identification of the central anomalous contrast that can be observed in Figure 8. The synthetic model 3 presented in this work is based on a rift-type basin with a density contrast of $-300\,kg/cm^3$ as illustrated in Figure 10. The inversion of the basin's gravimetric data was performed only with smoothness regularization for both density and depth contrast. The predicted data for depth and density contrast are shown in Figure 11 and it is possible to observe that at the edges of the basin, the adjustment is not as reliable as in the central region for the density contrast, in addition to the fact that the faults to the west of the basin are smoothed on inverted data. The graph in Figure 12 illustrates the fit between observed and calculated data through inversion.

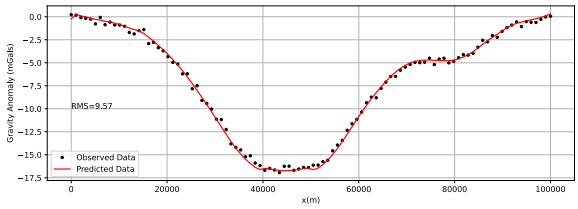

Figure 9: The graph presents the observed data (points) and calculated (red line) obtained through the regularized inversion of smoothness of the density contrast and for depth and with the regularization of a priori information of the density contrast related to model 2.

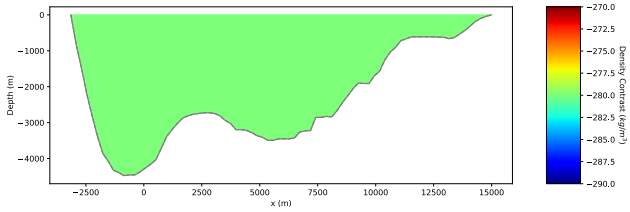

Figure 10: Model 3 of a synthetic rift basin with density contrast between the basement and the sediment of $-300\,kg/cm^3$.

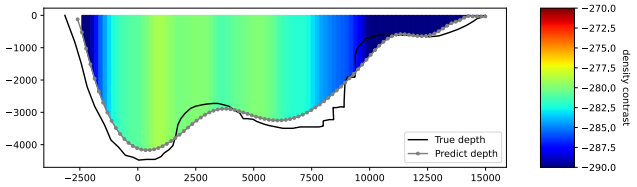

Figure 11: Density contrast data and basin depth of model 3 obtained through smooth inversion.

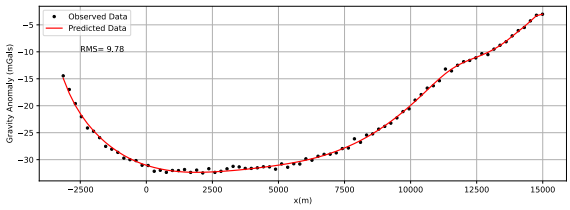

Figure 12: The graph presents the observed data (points) and calculated (red line) obtained through the smoothness regularized inversion of the density contrast and for depth related to model 3.

Conclusions

In comprehensive bibliographies, the gravimetric inversion for mapping the depth of the density contrast uses only the basin's depth as an inversion parameter, setting a constant value of the density contrast. The proposal presented in this work considers both the depth and the density contrast as input parameters, thus enabling mapping closer to reality since there is a complexity of the lateral geology that causes the variation in the density of the sedimentary layer.

Regularization by smoothing depth and density contrast was implemented to invert the first model. The results obtained for the first model were satisfactory, representing the real model well. Two inversions were performed for the second model, with depth smoothness and density contrast. Still, the second inversion included a priori data in the central region with anomalous density contrast. The first inversion of the second model, despite identifying a possible difference in density contrast in the center of the basin, did not identify as well as the second model with a priori information; this reaffirms the importance of a priori information provided by another geophysical methodology or by wells. The third basin model represents a rift-type basin with basement geology related to the depth parameter, which is more complex than the previous basins; the results, despite being satisfactory, were less reasonable than the earlier models. Observing a more significant smoothing in-depth and a difference in density contrast at the basin's edges is possible.

Finally, the applied geophysical inversion methodology to calculate a sedimentary basin's depth and density contrast presented satisfactory results. Implementing regularizations, both for smoothness and for a priori data, proved promising and convincing. The work could be expanded to more than one interface, generating predicted data for several layers within a sedimentary basin and the possibility of application in real data.

References

Bastos, B. M. S., Oliveira Jr, V. C. (2019). Isostatic constraint for 2D nonlinear gravity inversion on rifted margins. Geophysics, 85(1), G17-G34.

Barbosa, V. C. F., Silva, J. B., Medeiros, W. E. (1997). Gravity inversion of basement relief using approximate equality constraints on depths. Geophysics, 62(6), 1745-1757.

Barbosa, V. C., Silva, J. B., Medeiros, W. E. (1999). Stable inversion of gravity anomalies of sedimentary basins with nonsmooth basement reliefs and arbitrary density contrast variations. Geophysics, 64(3), 754-764.

Gòmez-Ortiz, D., Agarwal, B. N. (2005). 3DINVER. M: a MATLAB program to invert the gravity anomaly over a 3D horizontal density interface by ParkerâOldenburg's algorithm. Computers geosciences, 31(4), 513-520.

Silva, J. B., Oliveira, A. S., Barbosa, V. C. (2010). Gravity inversion of 2D basement relief using entropic regularization. Geophysics, 75(3), I29-I35.

Uieda, L., Barbosa, V. C. (2017). Fast nonlinear gravity inversion in spherical coordinates with application to the South American Moho. Geophysical Journal International, 208(1), 162-176.

Uieda, L. (2020). Short course on geophysical inversion at RWTH Aachen University graduate school IRTG-2379 Modern Inverse Problems. Department of Earth, Ocean and Ecological Sciences, School of Environmental

Sciences, University of Liverpool, UK.

Acknowledgments

We thank the National Institute of Science and Technology - Petroleum Geophysics (INCT-GP) for the availability of the essential research grant for developing this research. We thank the Federal University of Bahia (UFBA) for making its structure available for developing this research.